Development of a simulator of a satellite-to-satellite interferometer for determination of the Earth's gravity field

Shigeo Nagano,[a] Mizuhiko Hosokawa, Hiroo Kunimori, and Taizoh Yoshino
National Institute of Information and Communications Technology, Koganei, Tokyo 184-8795, Japan

Seiji Kawamura
National Astronomical Observatory of Japan, Mitaka, Tokyo 181-8588, Japan

Masashi Ohkawa and Takashi Sato
Faculty of Engineering, Niigata University, Ikarashi, Niigata 950-2181, Japan

(Received 7 March 2005; accepted 17 October 2005; published online 14 December 2005)

A satellite-to-satellite laser interferometer is essential for a future gravity-field mission to improve the accuracy and spatial resolution of the Earth's gravity model. We have designed a ground-based simulator of a satellite-to-satellite interferometer, which aims to evaluate instrument error reflecting on the accuracy of the gravity-field retrieval and achieve the essential technologies required to measure the intersatellite range rate. The developed simulator was successfully operated with a range-rate sensitivity of 40 $\mathrm{nm/s/\sqrt{Hz}}$ in the measurement band of 10^{-2}–1 Hz. From a primary demonstration, it was confirmed to be available for experimental simulation of the satellite-to-satellite interferometer in the laboratory. The simulator will be a powerful tool for establishing guidelines for the development of future gravity missions. © *2005 American Institute of Physics.* [DOI: 10.1063/1.2140280]

I. INTRODUCTION

Improving the accuracy and spatial resolution of the gravity field is expected to reveal new aspects of the Earth's system and result in advances in geodesic positioning ultimately limited by the precision of the present model of global gravity. Innovative satellite gravity missions are recently started or scheduled to measure the global gravity field with high accuracy.[1–3] The principle of these missions is to continuously track the free-fall motion of a satellite within a low Earth orbit from Global Positioning System (GPS) satellites at different altitudes and orbit inclinations: satellite-to-satellite tracking in the high-low mode (SST-HL).[4] Nongravitational forces acting on the satellite are distinguished from gravity-field signals by precision accelerometers located in the spacecraft's center of mass. Satellite laser ranging (SLR) also provides an auxiliary method for absolute gravity determination by measuring the accumulated orbit perturbations. Although these methods can estimate the long-wavelength part of the gravity field precisely, the medium- and short-wavelength parts are hardly determined. To enhance medium- and short-wavelength gravity signals as well as to improve the long-wavelength accuracy, the range-rate measurement between two satellites in tandem formation (satellite-to-satellite tracking in the low-low mode, SST-LL)[5] and the differential gravity measurement in the spacecraft (satellite gravity gradiometry)[6] are employed.

The Gravity Recovery and Climate Experiment (GRACE) was launched for mapping the global gravity field with an accuracy of 1 cm and a spatial resolution of 350 km.[7] The GRACE mission has significantly improved the global gravity model and has observed monthly geoid variations that have been attributed to water mass distribution.[8] These results were achieved with the SST-LL method using a microwave-ranging system.[9] However, a more accurate static gravity-field model and further information on temporal geoid variations are needed not only for practical applications but expansion of our knowledge regarding various dynamic processes of Earth's system.

A future satellite gravity mission is proposed in Japan.[10] The mission goal is to detect a geoid with millimeter-level accuracy and a spatial half-wavelength resolution of 100 km. The mission also aims to observe the time-variant geoid amplitude. The concept of the mission is illustrated in Fig. 1. Two satellites will be launched into a near-polar orbit at an altitude of 275 km to avoid attenuating the gravity signal, and will fly 50 km apart to resolve the gravity field at the targeted resolution in space. There will be several scientific instruments indispensable to attain the mission goal. Among them, a satellite-to-satellite laser interferometer (SSI) is anticipated as a key instrument. It measures variations in the intersatellite range rate by laser interference; the lead satellite will contain a laser and photodiode for tracking the passive trailing satellite. The SSI provides higher range-rate sensitivity than a microwave-ranging system. Besides, the SSI method also has two other advantages: it is a miniaturized ranging instrument that will enable the mission to be carried out using microsatellite buses, and has low power consumption, which will enable the mission lifetime to be extended.

Numerical simulations are likely to be powerful tools that provide information for the conceptual design of future missions. In fact, numerical simulations have been per-

[a]Electronic mail: nagano@nict.go.jp

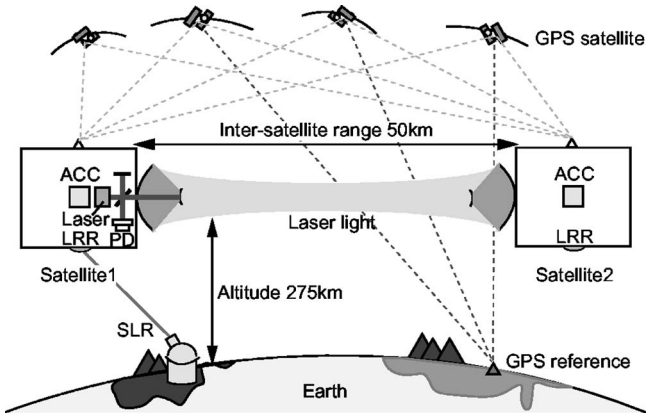

FIG. 1. Concept for satellite gravity mission proposed in Japan. Two satellites in a near-polar orbit of 275 km altitude fly 50 km apart. The global positioning system (GPS) continuously tracks the satellite motion for the SST-HL. Precision accelerometers (ACCs) measure the nongravitational disturbing forces acting on the satellites. A satellite laser ranging (SLR) also determines the satellite orbit using laser-retro reflectors (LRRs). A laser interferometer detects changes in the relative velocity between the twin satellite. A laser and photodiode (PD) are contained in the lead satellite 1. The laser beam emitted from this satellite is directly reflected by the following satellite 2.

formed to assess many different missions projected.[11–15] Their scientific instruments were assumed to have the simple white noise or comprehensive noise in the simulations. On the other hand, many scientific instruments for future missions, which include the relevant components of the laser interferometric space antenna,[16] have been demonstrated with excellent performance as elements of an overall system.[17–21] Nevertheless, experimental simulation with a laboratory apparatus, which corresponds closely to the mission concept, has not been addressed to ensure the feasibility of the mission.

In this article, we present a ground-based simulator of a SSI for a future satellite gravity mission having the potential to determine the Earth's gravity field with unprecedented accuracy. The simulator was designed to study the gravity-field retrieval from the SSI output in an experimental simulation and to investigate the major technologies related to the attainment of the SSI sensitivity required. From a demonstration of a gravity signal injection, the developed simulator was found to be available for assessment of the SSI method from the viewpoint of geoid error in a laboratory. It enables us to obtain guidelines that can be used in developing future missions.

II. CONCEPTUAL DESIGN OF GROUND-BASED SIMULATOR FOR SSI

The conceptual design of the ground-based simulator for a satellite gravity mission using the SSI method is illustrated in Fig. 2. There are three elements to be simulated: the Doppler frequency shift, optical path-length difference, and differential light power.

The effect of the disturbing geopotential on a mirror fixed on the following satellite 2 results in the relative motion to a beam splitter in the primary satellite 1. The frequency of the laser beam in the measurement arm is shifted by $2\nu u(t)/c$ due to the Doppler effect, where ν is the laser

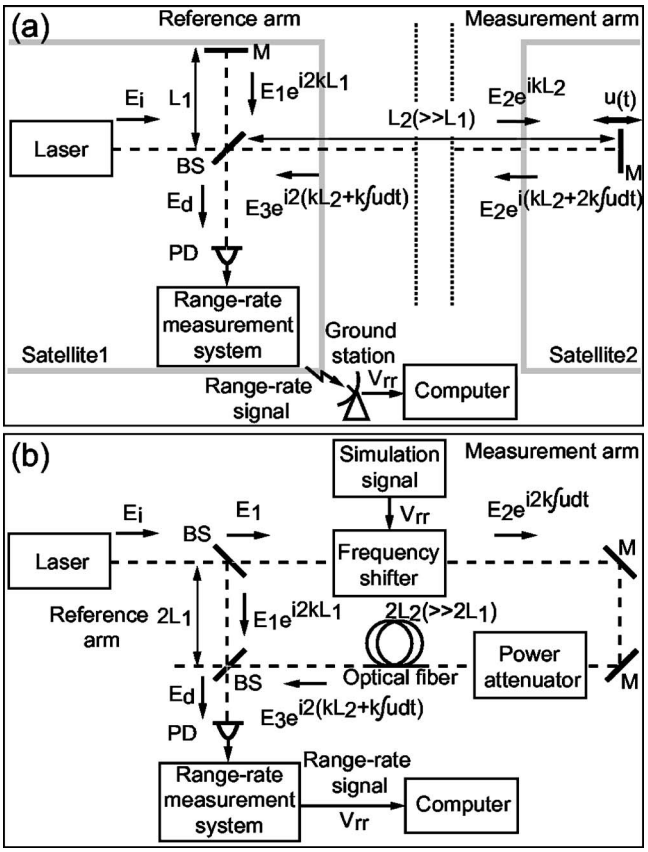

FIG. 2. (a) Optical layout of SSI for satellite gravity mission and (b) conceptual design of ground-based simulator for SSI. This apparatus simulates the laser Doppler frequency shift, optical path-length difference, and differential light power. *E*: light field, V: voltage, $u(t)$: velocity, *L*: interferometer arm length, *k*: wave number, BS: beam splitter, M: mirror, and PD: photodiode.

frequency, c is the speed of light, and $u(t)$ is the relative velocity between the two satellites. The frequency shift is expected to reach up to 300 kHz, since the maximum inter-satellite range rate is predicted to be 15 cm/s in the planned orbit with an eccentricity of 5.0×10^{-4}.[22] The SSI sensitivity must be 10 nm/s/$\sqrt{\text{Hz}}$ in the measurement band from 10^{-2} to 1 Hz.[23] Therefore, a range-rate measuring technique with a wide measurement range and high sensitivity in the low-frequency band is required to attain the mission goal. A Mach-Zehnder interferometer, which equips a frequency shifter in one arm, was employed in the simulator design. This configuration is suitable for experimental simulation of gravity-field retrieval and the development of the measuring technique. The frequency shifter generates a pseudo-Doppler frequency corresponding to the motion of the mirror, hence a phase term $2k\int udt$ can be added relative to the input field, where k is the wave number.

The output beam of the interferometer is used for the detection of the range-rate signal. Laser frequency noise also appears in the interferometer output as a spurious signal coupling with the optical path-length difference of the interferometer arms, since the large asymmetry of the SSI is unavoidable owing to the mission design. When the laser frequency ν consists of the carrier ν_0 and noise component $\delta\nu$, the photocurrent I_d on a photodiode (PD) is written as

$$I_d = |E_d|^2 = \frac{|E_1|^2 + |E_3|^2}{4}\left[1 + \frac{2|E_1 E_3^*|}{|E_1|^2 + |E_3|^2} \times \cos\left(\frac{4\pi\nu_0}{c}\Delta L + \frac{4\pi\delta\nu}{c}\Delta L + 2k\int udt\right)\right], \quad (\delta\nu/\nu_0 \ll 1), \quad (1)$$

where E_d is the field amplitudes of detected beam. E_1 and E_3 are the field amplitudes returning from each arm, respectively. ΔL is the static arm-length difference of the interferometer. We assumed the amplitude reflectivity of the mirrors (Ms) was unity and the beam splitters (BSs) were 50/50 in reflectivity/transmissivity. The quantum efficiency of the PD was also assumed to be unity for convenience. The second term of the cosine represents the spurious signal mentioned above, whereas the first and third terms represent the static phase and range-rate signal components, respectively. In the ground-based simulator, an optical fiber is placed in one arm to introduce an optical path-length difference $2L_2$. This changes the relative phase of interfering light beams by multiplying the light amplitude of the measurement arm by $\exp(i2kL_2)$. Consequently, it enables us to investigate the influence of the frequency noise on the SSI sensitivity, which is reflected in the geoid error. The simulator also serves as a test bench for frequency-stabilized lasers developed for the space mission.

The diffraction loss of the received beam at the far satellite is inevitable for the beam divergence governed by the finite size of the receiving and transmitting telescopes. The loss degrades the contrast of the interferometer output due to the power differential in the arms of interferometer. This results in the increasing of the shot-noise level as well as the mixing of various noise in the range-rate signal for the signal-to-noise ratio decreased. In the simulator, a power attenuator is set in the measurement arm to operate the interferometer with arbitrary power differential. Thus, the simulator is available to restrict an allowable size of the telescope in terms of the geoid error.

Other noise also influence on the precise range-rate measurement by a combination of various imperfections in the interferometer. They must be reduced by active stabilization systems, otherwise they should be effectively rejected from the range-rate signals measured. Automatic alignment control is essential to ensure stable operation of the SSI with the required sensitivity, because the beam geometrical fluctuation caused by the satellite attitude changes would produce critical noise in the measurement and degrade the robustness of SSI operation. The simulator provides a suitable environment for developing an alignment control system.

III. DETAILED DISCRIPTION OF GROUND-BASED SIMULATOR

The ground-based simulator we developed consists of three main systems: an interferometer, a frequency-stabilized laser, and an automatic alignment controller. This is because the simulator must be stably operated with sufficient sensitivity for signal-injection simulation to study the retrieval of gravity signals. Additionally, the simulator is required to provide a test bench for assessing the technologies that need to be developed for attainment of the SSI sensitivity aimed: interferometric range-rate measurement, laser frequency stabilization, and satellite attitude control.

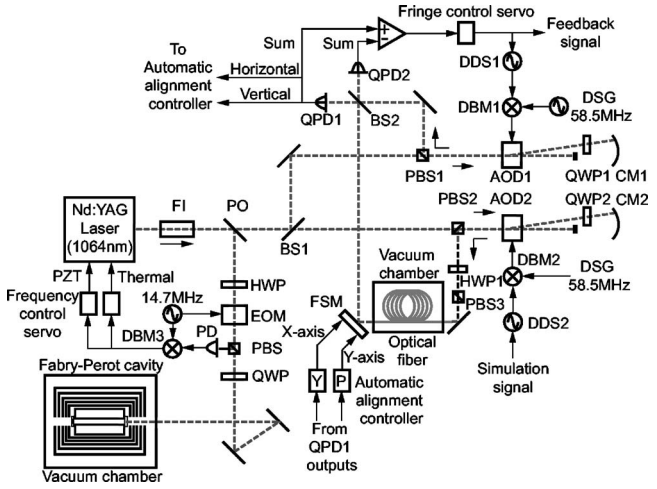

FIG. 3. Schematic diagram of ground-based simulator. It consists of an interferometer, frequency-stabilized laser, and automatic alignment controller. FI: Faraday isolator, PO: pick-off plate, BS: beam splitter, CM: concave mirror, HWP: half wave plate, QWP: quarter wave plate, AOD: acousto-optic deflector, EOM: electro-optical modulator, FSM: fast-steering mirror, PD: photodiode, QPD: quadrant photodiode, DDS: direct digital synthesizer, and DSG: digital signal generator.

A. Interferometer

A schematic diagram of the ground-based simulator is illustrated in Fig. 3. We employed a modified Mach-Zehnder interferometer with frequency shifters in each arm. The inline arm of the interferometer serves as a measurement arm, in which a frequency shifter is equipped as a simulation signal generator. It shifts the laser frequency by the Doppler frequency corresponding to the mirror velocity; a mechanically moving mirror is not practical to generate the required Doppler shift by its displacement. The perpendicular arm is a reference arm. Its frequency shifter tunes the laser frequency to lock the interferometer at the half-bright fringe using a feedback control loop.

The frequency shifter is composed of an acousto-optic deflector (AOD), a quarter-wave plate, and a concave mirror. The laser beam is modulated in frequency by the AOD (Brimrose: TEM-80-2-1064). A double-pass configuration is adopted with the concave mirror to cancel the resultant changes in the diffraction angle by the frequency modulation. The quarter-wave plate rotates the polarization angle to separate incident and reflected beams.

The light reflected from the measurement arm is transmitted through a power attenuator. It comprises a half-wave plate (HWP 1) and polarizing beamsplitter (PBS 3) to adjust the light power difference between the reference and measurement arms. The maximum attenuation of the transmitted beam is more than 30 dB in power, which is limited by an extinction ratio of the PBS 3.

The attenuated beam is introduced into a polarization-maintained single-mode optical fiber with 998 m in length (Fujikura, SM 98-PS-U 25A). It is bundled on a reel, which is suspended by a single pendulum placed in a vacuum

chamber to prevent the fiber length fluctuations induced by seismic motion and temperature changes. Although this artificial optical path-length difference is two orders smaller than the supposed one, the influence of laser frequency noise on geoid error could be still investigated in the experimental simulation.

The measurement beam, which simulates the Doppler frequency shift, differential light power, and optical phase delay, is superimposed with a reference beam on a beam splitter 2(BS 2). A Doppler fringe is formed on two quadrant photodiodes (QPD 1 and QPD 2), and their sums of all the quadrants are used to extract the signal for the fringe-control servo. A balanced detection scheme is employed to effectively remove the laser intensity noise from the control signal. The signal is appropriately filter amplified by the servo electronics and then directed towards a voltage-frequency converter for driving the frequency shifter in the reference arm. The Doppler frequency-to-voltage conversion for the range-rate measurement is done by directly reading out the feedback signal to the voltage-frequency converter. Details of this measuring technique are described in our previous paper.[21]

The voltage-frequency converter consists of a direct digital synthesizer 1 (DDS 1), a digital signal generator (DSG), and a double-balanced mixer 1 (DBM 1). The outputs of the DDS 1 generator at a center frequency of 19 MHz and the DSG at a fixed frequency of 58.5 MHz are upconverted by the DBM 1 to produce a carrier at 77.5 MHz for driving the AOD 1. The DDS 1 generator is a key device in the voltage-frequency converter (Digital Signal Technology, FIX-20 SP 1). Its output frequency can be phase continuously tuned around the center frequency by a control voltage applied through an analog-to-digital (A/D) converter with a 16 bit resolution. The output frequency range and resolution are set to be 762.839 Hz and 11.64 mHz, respectively. The pseudo-Doppler frequency for the signal-injection simulation should not exceed this range to maintain the interferometer operation. The DDS 1 generator is designed to have an update time for a new frequency within 140 μsec and a phase delay of less than 150° at a Fourier frequency of 1 kHz. This is because a digital-servo loop with a wide control bandwidth is needed to achieve the required feedback gain. The required gain is more than 200 dB at 0.18 mHz to suppress residual fluctuations around the locking point within 1/100 of the laser wavelength. This was decided considering the maximum range rate predicted, which will degrade the feedback-loop performance with the insufficient feedback gain.

The simulation signal generator is also driven by another voltage-frequency converter, which is represented by a set of DDS 2, DSG, and DBM 2. It can produce simulation signals with a resolution of 12 nm/s at the relative velocity between the twin satellite. For signal-injection simulation, an analog wave form is generated by a digital-to-analogue (D/A) converter (maximum 333 kilosamples/s, 16 bit) on a multifunction data-acquisition board (National Instruments, PCI-6052 E) controlled by softwares written using LABVIEW.[24] The signal wave form reconstructed in the feedback signal of the fringe-control loop is recorded through an A/D converter (maximum 333 kilosamples/s, 16 bit) placed on the same board after passing through an antialiasing filter.

B. Frequency-stabilized laser

Laser frequency noise appears in the interferometer output as a spurious range signal coupled with the asymmetry of the interferometer. The range signal δx has the following well-known relationship with the frequency noise: $\delta x = \Delta L \delta \nu / \nu$. In the range-rate signal, the range signal is differentiated, and thus the original signal is multiplied by an angular frequency. Accordingly, the required frequency stability is given by

$$\delta \nu = \frac{\nu}{2\pi f \Delta L} \delta v, \tag{2}$$

where δv is the aimed range-rate sensitivity and f is a Fourier frequency. In our simulator development, the frequency noise must be suppressed below $450/f$ Hz/$\sqrt{\text{Hz}}$ between 10^{-2} and 1 Hz assuming the aimed δv of 10 nm/s/$\sqrt{\text{Hz}}$ and $\nu = 282$ THz. It should be ultimately reduced to $9/f$ Hz/$\sqrt{\text{Hz}}$ because of the arm-length difference of 50 km in the SSI. Although the differential process relaxes the requirement for the frequency stability toward the lower frequency, a highly stable frequency reference and feedback-control system are essential to satisfy the requirement. A space-qualified design must also be considered when choosing the light source and its frequency stabilization technique.

The light source we employed is a laser-diode-pumped monolithic Nd: yttrium aluminum garnet (YAG) laser with an output power of 200 mW [nonplanar ring oscillator (NPRO), Innolight, Mephisto 200 NE]. It generates single frequency, linear-polarized, TEM_{00} oscillation with low intrinsic noise. The Pound-Drever-Hall technique with phase modulation at 14.7 MHz is used to extract the control signal for the laser frequency.[25] The frequency reference is a Fabry-Pérot cavity consisting of two highly reflective mirrors and an ultralow-expansion (ULE) glass ceramic spacer inserted between them (Research Electro-Optics, ULE-100). Its free-spectral range and finesse are 1.5 GHz and 110 000, respectively. The cavity is covered by a five-layer thermal shield made from reflective optically coated aluminum sheets, which is set in a vacuum chamber kept at 1.6×10^{-3} Pa for isolating the cavity from fluctuations in the environmental temperature and acoustic disturbance.[26] The control topology is designed to maintain stable frequency locking and achieve the frequency-noise level required. The control signal is fed back to two actuators of NPRO: a thermal and piezoelectric transducer (PZT) tuning. The low- (below 0.1 Hz) frequency components of the signal are fed back to the thermal tuning with wide control range and slow response for the compensation of large frequency drifts. The high- (0.1–50 kHz) frequency components are directed toward the PZT tuning with fast response and narrow control range for expansion of the control bandwidth. The control system was optimized using a computer simulation, then an open-loop gain of 80 dB below 1 Hz was achievable with this control topology. This gain is large enough to suppress the free-running frequency noise to the final required level.

C. Automatic alignment controller

Laser beam jitter caused by changes in the satellite attitude results in apparent range variation by combination of the wave front distortion due to the imperfections in the optical components. Similar results about this mechanism have been reported by other researchers.[27,28] The range-rate variation is given by the multiplication of the range variation by the angular frequency, as mentioned above. As reported by Robertson *et al.*, the required beam jitter $\delta\theta$ is derived as

$$\delta\theta = \left(\frac{2\lambda}{D}\right)^2 \frac{1}{\pi^3 d\theta_{\mathrm{dc}}} \frac{\delta v}{f}, \tag{3}$$

where λ is the laser wavelength, d is the amplitude of mirror curvature error, D is the mirror diameter and θ_{dc} is the root-mean-square (rms) fluctuation of beam pointing. If $\lambda = 1064$ nm, $d = \lambda/10$ m, $D = 30$ cm, and $\theta_{\mathrm{dc}} = 10^{-5}$ rad are assumed, the beam jitter must be reduced to less than $\delta\theta = 0.15\ \mu\mathrm{rad}/\sqrt{\mathrm{Hz}}$ at 0.1 Hz. However, the design of an overall control topology satisfying the requirement is difficult at present, because the satellite-bus design and surface force effect on the satellite orbit have not been researched in detail; the contribution from these factors will strongly reflect the satellite attitude variations in the space environment. Thus, developing a signal extraction scheme for automatic alignment control became the major focus of using the ground-based simulator rather than design and development of the overall system.

Alignment control signals are obtained by the wave-front sensing scheme.[29] The beam geometrical fluctuation is regarded as the mixing of higher-order modes to a TEM_{00} mode. This mixing forms different interference patterns between vertical/horizontal pairs of QPD 1's segments by interfering with another fundamental mode as a reference. The signals subtracted the outputs of each segments pair are used for the alignment control of the pitch and yaw motions. To suppress the beam jitter, the control signals obtained are fed back to a fast-steering mirror (FSM, Newport, FSM-200) in the measurement arm. It is actuated by voice coils producing two orthogonal rotations about the horizontal and vertical axes. The FSM has an angular range of 52.4 mrad and a flat frequency response of up to around 700 Hz. This automatic alignment controller is available to maintain the stable long-term operation of the interferometer as well to evaluate the signal extraction scheme developed.

IV. PERFORMANCE OF THE GROUND-BASED SIMULATOR

A. Interferometer

To provide the performance of the developed simulator, the interferometer was operated without the power attenuator. The power ratio between the reference and measurement beam was 1.2 in this operation, although the power differential of 2.9 is expected with a Gaussian beam optimized for 50 km transmission between the telescope mirrors of 30 cm in diameter. This difference does not affect the overall performance of the simulator because the proper operation of the simulator is confirmed with much larger power differential as described in the next section.

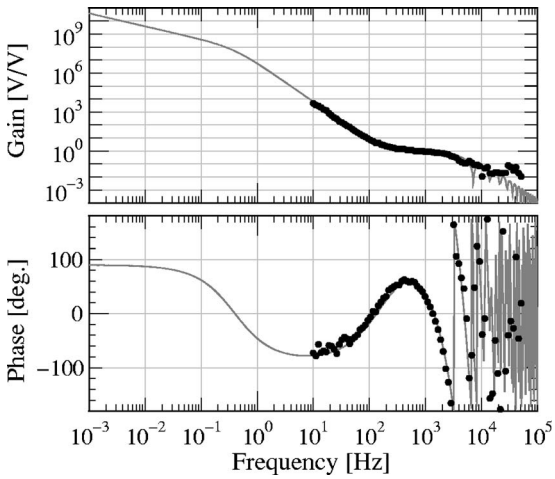

FIG. 4. Measured open-loop transfer function of fringe-control loop. The bold line and dots represent the calculated and measured open-loop transfer function of the fringe-control loop.

Figure 4 plots the measured open-loop transfer function of the fringe-control loop. The unity gain frequency and phase margin were measured to be about 1 kHz and 35°, respectively. The control bandwidth is limited by the sampling frequency of the A/D converter for tuning the output frequency of the DDS generator. The achieved feedback gain of 200 dB below 4 mHz is satisfying the requirement. The dips in the gain curve at 7.1 Hz and its harmonics originate from the transfer function of the A/D converter.

The range-rate sensitivity of the interferometer was measured to be 40 $\mathrm{nm/s}/\sqrt{\mathrm{Hz}}$ at the measurement band as shown in Fig. 5. It was estimated from the feedback signal to the voltage-frequency converter. This sensitivity will impose a limitation on the accuracy of gravity recovery in the experimental simulation. The laser power on each QPD was about 0.2 mW after being attenuated using a neutral density filter. The shot-noise level corresponding to the photocurrent was calculated to be $5.4\times10^{-14} f\ \mathrm{m/s}/\sqrt{\mathrm{Hz}}$. The present sensitivity is mainly dominated by the phase noise of the DDS gen-

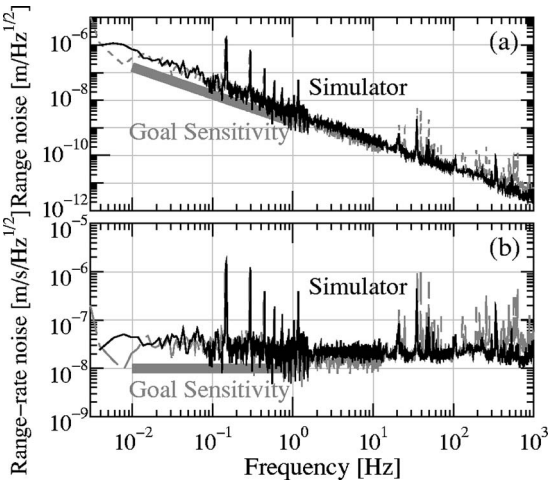

FIG. 5. (a) Range noise spectrum and (b) range-rate noise spectrum of Mach-Zehnder interferometer. The black solid and gray dashed lines represent the noise spectra with the power differential of 1.2 and 10^3 in the interferometer arms, respectively. The goal sensitivity of the SSI for the Japanese satellite gravity mission is also indicated by the gray line.

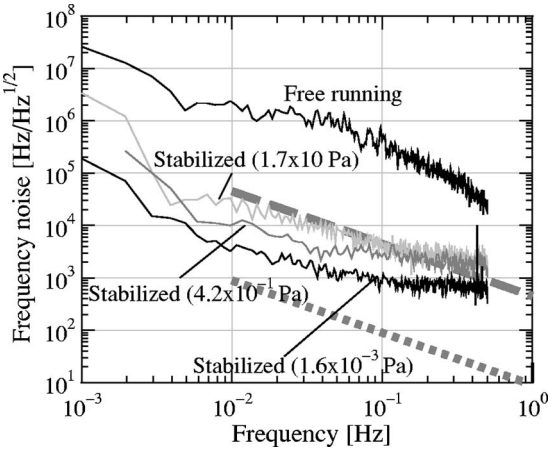

FIG. 6. Frequency-noise spectra of light source for ground-based simulator. The top and bottom traces indicate the free-running frequency noise and the frequency noise of the stabilized light source. The traces indexed with different pressures represent the frequency noise of the light source referenced to the Fabry-Pérot cavity at each pressure. The required noise levels for the ground-based simulator and Japanese satellite gravity mission are also indicated by the dashed and dotted lines, respectively.

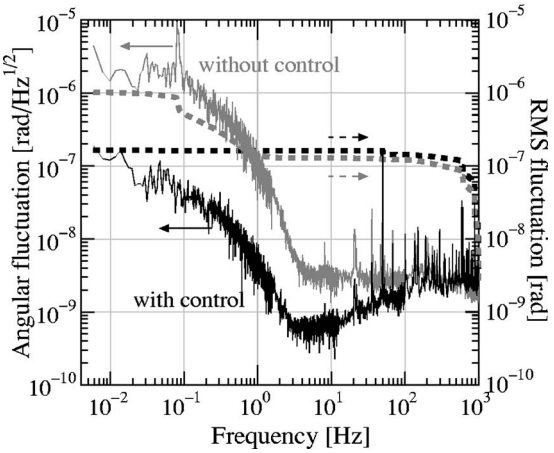

FIG. 7. Estimated angular fluctuation spectra of laser beam and rms fluctuations (pitch motion). The black and gray solid lines represent the angular fluctuation spectrum with/without alignment control. The black and gray dotted lines are their rms fluctuations.

erator in the voltage-frequency converters and the air density variations propagating to the optical components. The noise sources appearing in the interferometer output is discussed in Sec. VI in detail.

The measurement range is restricted by the output frequency range of the DDS 1 generator for driving the frequency shifter in the reference arm. The achievable frequency shift corresponds to 0.8 mm/s in the intersatellite range rate. Therefore, any satellite motion within this allowable range rate can be simulated with the attained sensitivity. The extension of the measurement range is discussed in a later section.

The interferometer was operated over 10 h without degradation of the sensitivity. The fringe lock was acquired immediately after feeding back the control signal to the voltage-frequency converter, even though a high-frequency Doppler fringe appeared in the interferometer output. These features of the interferometer are important in an experimental simulation, because they ensure the remeasurement without a serious delay after the interrupted operation of the interferometer.

B. Frequency-stabilized laser

Absolute optical frequency measurements were implemented to asses the performance of the frequency-stabilized laser developed. We measured the beat frequency between the stabilized laser and a femtosecond mode-locked laser referenced to a microwave clock with a stability of $\sim 10^{-13}$ between 1 and 100 s in the square root of the Allan variance.[30] In Fig. 6, the lowermost trace indicates the frequency-noise spectrum calculated from the beat frequency. The measured noise level was 700 Hz/$\sqrt{\text{Hz}}$ at 0.2 Hz, which corresponds to 9×10^{-13} in the Allan variance. As compared with the stability of the mode-locked laser, it obviously exhibits the frequency-noise spectrum of the stabilized laser. The chamber containing the reference cavity was evacuated at 1.6×10^{-3} Pa during the measurement. The uppermost trace indicates the frequency-noise spectrum of the NPRO in the free-running state for comparison. The light power on the PD was about 100 μW and the shot-noise level was calculated to be 2×10^{-4} Hz/$\sqrt{\text{Hz}}$.[31] The frequency-noise stabilized poses no significant limitation on operating the ground-based simulator at the goal sensitivity.

The control bandwidth of the servo was measured to be approximately 52 kHz, and thus the open-loop gain was attained to be more than 150 dB below 1 Hz. It is sufficient to accomplish the ultimately required stability. This frequency-stabilized laser has the potential to be employed for a satellite gravity mission in terms of the noise performance. Other components of the performance, particularly those that depend on the space environment, should be checked using an engineering model of the stabilized laser system.

C. Automatic alignment controller

Figure 7 shows the angular fluctuation spectra of pitch motion, which were converted from the error signals of the alignment control loop. The fluctuated angle of the laser beam was 2 μrad/$\sqrt{\text{Hz}}$ at 0.1 Hz without the alignment control. The rms fluctuation in the region between 5 mHz and 1 kHz was calculated to be 1 μrad. With the alignment control, the fluctuated angle and rms fluctuation were suppressed to 40 nrad/$\sqrt{\text{Hz}}$ and 0.16 μrad, respectively. The angular fluctuation spectra of the yaw motion are also shown in Fig. 8. The fluctuated angle and the rms fluctuation were effectively reduced to 30 nrad/$\sqrt{\text{Hz}}$ at 0.1 Hz and 0.1 μrad by the alignment control loop for yaw motion. The unity gain frequency of both control loops was measured to be about 200 Hz. The alignment controller developed has successfully decreased the amplitude of the beam geometrical fluctuation. Consequently, the signal extraction scheme used in this study was demonstrated to be suitable for application in a future gravity mission using the SSI method in conjunction with the FSM. The developed controller was also shown to be suitable for stable long-term operation of the ground-based simulator during the demonstration described in the next section.

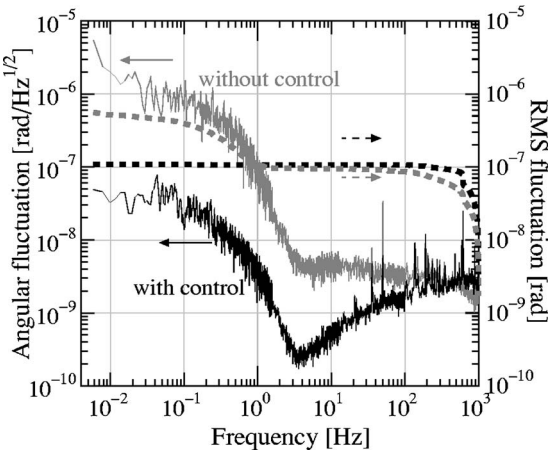

FIG. 8. Estimated angular fluctuation spectra of laser beam and rms fluctuations (yaw motion). The black and gray solid lines represent the angular fluctuation spectrum with/without alignment control. The black and gray dotted lines are their rms fluctuations.

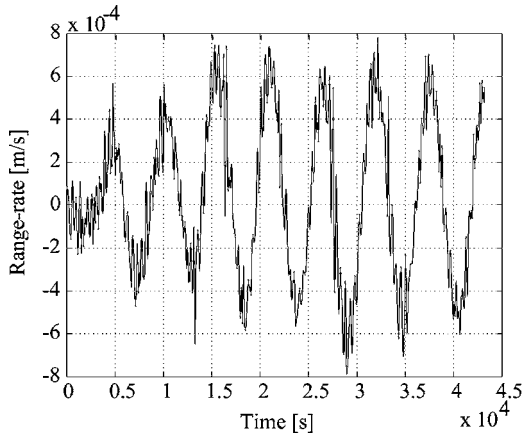

FIG. 9. Range-rate signal wave form for signal-injection simulation. This was computed using a satellite-orbit analysis software. Twin satellites were assumed to be flown in a near-polar orbit at an altitude of 450 km with an inclination of 89° and separated from each other by 50 km in the along-track direction. The geopotential model EGM 96 was used for the orbit analysis. For simplicity, the effect of nongravitational forces was neglected in the analysis.

V. DEMONSTRATION OF GROUND-BASED SIMULATOR

A. Signal-injection simulation

The procedure of the experimental simulation should be essentially consisting of two steps: (1) simulated signal injection and range-rate measurement using the instruments developed and (2) recovery of the global gravity field from the measured signals and evaluation of the geoid error propagated from the instrument noise. In practice, the measured signals must be taken over a fairly long period to guarantee enough measurements covering the entire sphere of Earth. The signals are appropriately averaged over each specific area on the sphere, and the averaged data in the space domain are converted to spherical harmonics in the spectral domain to obtain the geoid error. However, such an analysis is beyond the scope of this article. Therefore, only the first step was implemented for the demonstration of the ground-based simulator. The second step will be addressed in the next phase of this feasibility study of the SSI method in comparison with numerical simulations.

The range-rate signal wave form for the signal-injection simulation is shown in Fig. 9. It was computed by a satellite-orbit analysis software assuming the satellite altitude of 450 km, intersatellite separation of 50 km, and an orbit inclination of 89°.[32] It should be noted that the orbit altitude is not consistent with that described in Sec. I. The Earth's static geoid model EGM 96, whose spherical harmonic degrees over 70 were truncated, was utilized for the orbit analysis. To meet the measurement range of the ground-based simulator, the spherical harmonic degrees up to 11 were omitted for decreasing the maximum relative velocity of the satellites. The initial condition of the eccentricity was also set to zero for the same reason; consequently the demonstration was able to proceed without frequent interruptions. In addition, any nongravitational accelerations caused by atmospheric drag, radiation pressures from the Sun and Earth, etc., were neglected in the analysis for simplicity.

The range-rate signal wave form was appropriately calibrated and then generated by the D/A converter set by 200 Hz sampling. The signal wave form generated was applied to the simulation signal generator through the voltage-frequency converter so as to produce the relevant pseudo-Doppler shift. The power attenuator in the interferometer was not used in this experimental simulation. Figure 10 shows the residual noise of the range-rate signal reconstructed in the feedback signal with respect to the simulation signal injected. There exists no large deviation from the zero point. Therefore, it was found that the simulation signal was successfully recovered in the feedback signal without significant degradation. The amplitude of the residual noise was principally contributed by the frequency components of the interferometer noise below the measurement band. The large spike noise came from the computer mounting the multifunction data-acquisition board.

In Fig. 11, the dotted and solid lines indicate the spectrum of the original range-rate signal and that of the feedback signal during the signal-injection simulation. The spectrum of the original signal rapidly decreases toward the higher

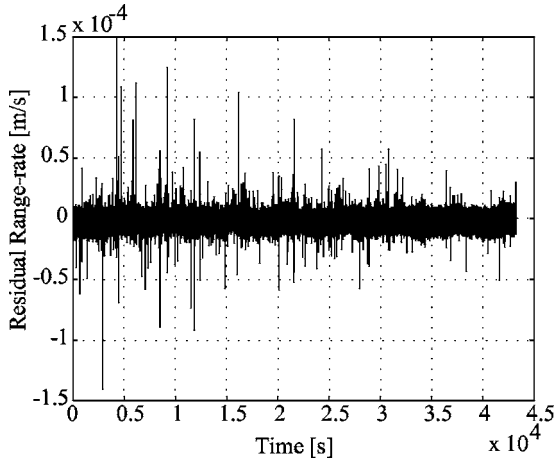

FIG. 10. Residual noise of range-rate signal retrieved. The original signal injected into the ground-based simulator was subtracted from the feedback signal of the fringe-control loop.

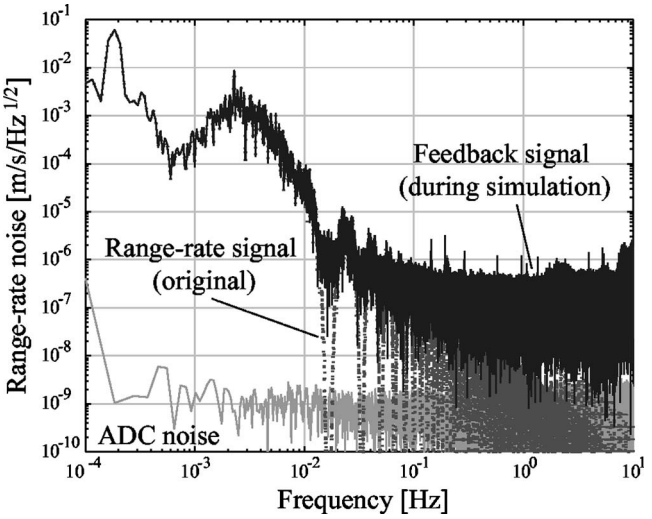

FIG. 11. Range-rate signal spectra. The dotted and solid lines indicate the spectrum of the original range-rate signal and that of the feedback signal during the signal-injection simulation, respectively. The spectrum of the analog-to-digital converter (ADC) noise is also shown by a gray line.

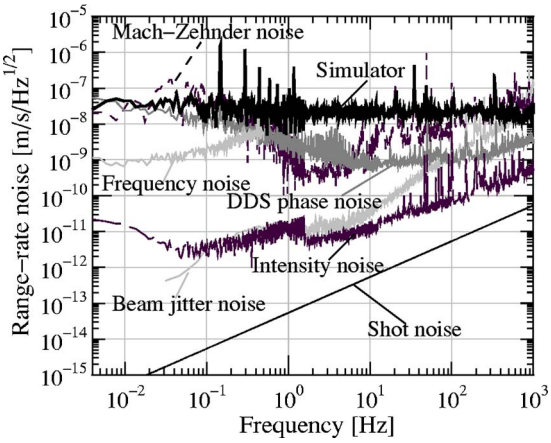

FIG. 12. Range-rate noise level of the ground-based simulator and the contribution of identified noise sources. The present sensitivity in the measurement band is restricted by the DDS phase noise and Mach-Zehnder noise.

frequencies, since high-frequency signal components, which are caused by the short-wavelength part of the Earth's gravity field, are intrinsically small within the satellite trajectories. The dips at 16 mHz and its harmonics might result in the truncation of the higher degree terms over 70 in the EGM 96. Below 0.3 Hz, the spectrum of the feedback signal is in a good agreement with that of the original signal. The ground-based simulator has the potential for the detection of the gravity signal components below the frequency. Hence, it was found to be available for an experimental simulation, which provides guidelines for the development of future missions. In contrast, the signal components above 0.3 Hz were buried in the interferometer noise and not registered in the feedback signal. Further improvement of the interferometer sensitivity is required to observe them.

B. Power-differential simulation

The power-differential simulation can give a criteria of the satellite-bus design. The power attenuator in the measurement arm allows the operation of the simulator with arbitrary power differential in the arms of interferometer. Thus, the ground-based simulator developed is suitable to decide the size of the receiving and transmitting telescope in the view of range-rate sensitivity required. The telescope mirror of 30 cm in diameter, which results in the power differential of only 2.9, was assumed in Sec. III to improve the shot-noise level and the mixing of noise in the signal. However, it is worthwhile to demonstrate the operation of the simulator with larger power differential.

The gray dashed lines in Fig. 5 represent the range and range-rate sensitivities of the interferometer with the power differential of 10^3. It corresponds to the case for the laser transmission of 50 km between mirrors of 11.7 cm in diameter. We observed no significant degradation of the sensitivity and stability at this level of the power differential. Therefore, it was found that the telescopes with 11.7 cm diameter are acceptable to the gravity mission we proposed. The light power in reference and measurement arms were 502 μW and 490 nW, respectively. The shot-noise level was calculated to be $2.1\times10^{-13}f$ m/s/$\sqrt{\text{Hz}}$, which was still lower than the sensitivity achieved.

For the stable operation of the alignment control, the control bandwidth must be decreased to be 70 Hz. This modification could be needed for the reduction of the influence of the laser intensity noise, since the signal-to-noise ratio of the alignment control signal was decreased toward the higher frequency. It will be essential to study a more efficient signal extraction scheme for the alignment control, if much smaller mirrors are planned to be employed for the telescopes.

VI. DISCUSSION

To improve the current sensitivity of the interferometer, the noise sources which limit the sensitivity should be identified. Figure 12 shows the typical noise budget of the ground-based simulator developed. The present sensitivity in the measurement band is mostly restricted by two noise sources: the phase noise of the DDS generator in the voltage-frequency converters (DDS phase noise) and the phase-detection noise of the Mach-Zehnder interferometer without two AODs (Mach-Zehnder noise). The influence of the DDS phase noise was revealed from a calibrated error signal of a phase-noise measurement, in which one DDS generator was phase locked to the other with a phase-locked loop. A peak at 0.14 Hz and its harmonics in the noise spectrum were also identified to result in the generator. To realize the designed sensitivity of the simulator, the DDS phase noise should be removed by replacement with DDS generators having lower phase noise. The Mach-Zehnder noise includes many noise sources such as the seismic noise, acoustic noise, length fluctuation of the optical bench, etc. The air density variations propagating to the optical components would dominate the Mach-Zehnder noise in the measurement band, since the noise level was increased with turning on the air conditioner in the laboratory. This noise can be reduced by hermetically shielding the optical components or putting them into a vacuum chamber. The Mach-Zehnder noise does not reflect

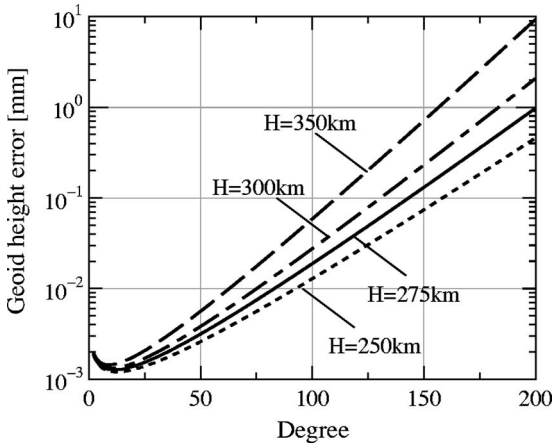

FIG. 13. Geoid height errors for different satellite altitudes: H=250, 275, 300, and 350 km. The intersatellite range is 50 km, the range-rate sensitivity is 10 nm/s, the mission duration is 60 days and the sampling interval is 5 s.

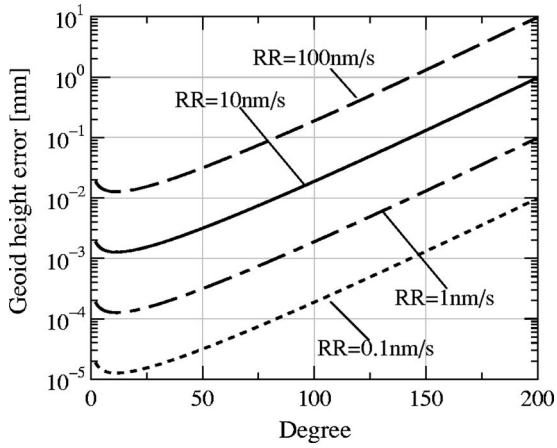

FIG. 14. Geoid height errors for different range-rate sensitivity: RR=0.1, 1, 10, and 100 nm/s. The altitude of the satellite orbit is 275 km. The other parameters are the same as in Fig. 13.

optical path-length fluctuations inside the AOD. The length fluctuation δL caused by the temperature fluctuation of the AOD are given by $\delta L = 2L(dn/dT)\delta T$, where L is the length of the AOD crystal, dn/dT represents the temperature coefficient of refractive index of the crystal, and δT is the temperature fluctuation. In tellurium dioxide (TeO2) used for our AODs, $L=30$ mm and $dn/dT=5.9\times10^{-6}$/K at 1064 nm,[33] the length fluctuation was estimated to be below 7.1 nm/$\sqrt{\text{Hz}}$ at 0.1 Hz with the measured temperature fluctuation of less than 20 mK/$\sqrt{\text{Hz}}$. The corresponding range-rate noise level was 2.2 nm/s/$\sqrt{\text{Hz}}$, which was still lower than the present sensitivity of the interferometer.

According to the numerical simulation, the maximum range rate between the twin satellite is predicted to be 15 cm/s in the planned orbit with an eccentricity of 5.0×10^{-4}. The corresponding Doppler frequency shift on the laser beam will be 300 kHz at a Fourier frequency of 0.18 mHz. The present measurement range of the ground-based simulator, which is restricted by the output frequency range of the voltage-frequency converter, is insufficient for the simulation of the SSI in the global Earth's gravity field. We think, however, that there are no obstacles to expand the measurement range. A two-loop control topology for the fringe-control loop could be employed for a wider measurement range and control bandwidth. For the voltage-frequency converter, an individual DDS generator with a 24 bit$\Delta\Sigma$ A/D converter could be utilized as an auxiliary frequency actuator instead of the DSG generator. Such a DDS generator allows to shift the laser frequency by more than 390 kHz at 0.18 mHz, although it has slow response compared with the another DDS generator for the sake of the higher resolution.

Typically, AODs generate an inevitable Doppler shift in the optical frequency by the radio frequency. For dealing with Doppler frequencies that approach zero, the AOD in the reference arm also serves to shift the optical frequency by the same frequency shifted in the simulation signal generator. It makes a different optical configuration from the mission concept, in which there is no frequency modulator in the measurement arm of the SSI. An alternative technique is to employ an additional AOD in the frequency shifter of the reference arm, which only cancels the optical frequency shifted by the radio frequency. This would enable the frequency modulator to be removed from the measurement arm.

The stabilized frequency noise imposes no significant limitations on the operating ground-based simulator at the desired sensitivity, however, it still does not meet the ultimate requirement for the proposed mission. In Fig. 6, traces indexed with different pressures were obtained by the beat frequency measurements in which the chamber for the reference cavity was evacuated at each pressure. The variations in the environmental temperature were propagated to the cavity due to the inadequate isolation, and thus appeared as the frequency noise. The ultimate requirement could be accomplished by the high vacuum in the chamber or installing an active temperature controller for the cavity. The employment of a small Fabry-Perot cavity with high finesse might also help to improve the frequency stability for the reduced sensitivity to environmental temperature changes.[34] These need to be investigated further to optimize the stabilized laser system for the planned gravity mission.

ACKNOWLEDGMENTS

The authors would like to thank I. Naito, T. Tsuda, and Y. Fukuda for their efforts in starting this project. We are also indebted to H. Ito and Y. Li for their support of the frequency stability measurements, and together with T. Kubo-oka, K. Yamamoto, and T. Otsubo for preparing the simulation signals. This work was supported by Special Coordination Funds for Promoting Science and Technology from the Ministry of Education, Culture, Sports, Science and Technology.

APPENDIX

The geoid height error of the satellite gravity mission employing intersatellite range-rate measurement can be calculated from Eq. (60) in Ref. 11. Figure 13 shows the geoid height errors for different orbit altitudes. To calculate the geoid errors, we assumed that the intersatellite range of 50 km, range-rate sensitivity of 10 nm/s, mission duration of 60 days, and sampling interval of 5 sec. In satellite geodesy,

the terrestrial gravity field is usually written by a series of spherical harmonics. The nth degree of the harmonic coefficient is associated with the spatial wavelength of $\Lambda=2\pi R_e/n$, where R_e represents the radius of the Earth. A mission having the satellites at an altitude of 275 km can detect the geoid with millimeter-level accuracy at degree 200, which corresponds to the spatial resolution with the wavelength of 200 km. The lower altitude of the satellite orbit improves the accuracy of the short-wavelength part of the gravity field, although the mission lifetime is reduced by the decay of the satellite altitude due to the atmospheric drag.

Figure 14 compares the geoid height errors for different sensitivities of the intersatellite range-rate measurement. The satellite altitude was assumed to be 275 km, and the other mission parameters were the same as described above. The improvement of the range-rate sensitivity has a linear effect on that of the geoid error.

[1] C. Reigber, P. Schwintzer, and L. Lühr, Boll. Geof. Teor. Appl. **40**, 285–289 (1999).
[2] GRACE Team, GRACE Science and Mission Requirements Document No. (SMRD), GRACE327-200 JPL D-15928, 1998 (unpublished).
[3] R. Rummel, G. Balmio, J. Johannessen, P. Visser, and P. Woodworth, J. Geodyn. **33**, 3 (2002).
[4] G. Seeber, *Satellite Geodesy*, 2nd ed. (Walter de Gruyter, Berlin, 2003).
[5] M. Wolff, J. Geophys. Res. **74**, 5295 (1969).
[6] R. Forward, *Proceedings of the International Symposium on The Use of Artificial Satellites for Geodesy and Geodynamics*, edited by G. Veis (National Technical University, Athens, 1974), p. 157.
[7] K. H. Ilk, *Towards an Integrated Global Geodetic Observing System*, edited by R. Rummel, H. Drewes, W. Bosch, and H. Hornik (Springer, Heidelberg, 2000), pp. 53.
[8] B. D. Tapley, S. Bettadpur, J. C. Ries, P. F. Thompson, and M. M. Watkins, Science **305**, 503 (2004).
[9] J. L. MacArthur and A. S. Posner, IEEE Trans. Geosci. Remote Sens. **GE-23**, 517 (1985).
[10] Y. Fukuda, T. Otsubo, T. Yoshino, and S. Okubo, *A new project of gravity mission studies in Japan* presented at IUGG2003, Sapporo, Japan, 2003 (unpublished).
[11] C. Jakeli and R. H. Rapp, Department of Geodetic Science, Ohio State University, Columbus, Report No. 307, 1980, http://www.ceegs.ohio-state.edu/gsreports/ (unpublished).
[12] B. E. Schutz, B. D. Tapley, J. B. Lundberg, and P. Halamek, Manuscr. Geod. **12**, 51 (1987).
[13] C. A. Wagner, J. Geophys. Res. **92**, 8147 (1987).
[14] G. Balmio, F. Perosanz, R. Rummel, N. Sneeuw, and H. Sunkel, Boll. Geof. Teor. Appl. **40**, 309 (1999).
[15] J. Kim, Ph.D. thesis, University of Texas, 2000.
[16] LISA Study Team, European Space Agency, Report No. ESA-SCI(2000)11, 2000 (unpublished).
[17] W. M. Klipstein, M. Mohageg, J. A. White, and B. C. Yang, *Proceedings of the 2001 IEEE International Frequency Control Symposium and PDA Exhibition* (IEEE, Seattle, WA, 2001), p. 108.
[18] P. L. Bender, J. H. Hall, J. Ye, and W. M. Klipstein, Space Sci. Rev. **108**, 377 (2003).
[19] O. Jennrich, R. T. Stebbins, P. L. Bender, and S. Pollack, Class. Quantum Grav. **18**, 4159 (2001).
[20] G. Heinzel *et al.*, Class. Quantum Grav. **20**, 153 (2003).
[21] S. Nagano, T. Yoshino, H. Kunimori, M. Hosokawa, S. Kawamura, T. Sato, and M. Ohkawa, Meas. Sci. Technol. **15**, 2406 (2004).
[22] T. Otsubo (private communication).
[23] The gravity signal below 10^{-2} Hz will be measured by the SST-HL using GPS satellites. The signals from the SSI and SST-HL will be appropriately combined to estimate the gravity field of the entire Earth.
[24] LABVIEW6.1 (National Instruments Corporation, 2001).
[25] R. W. P. Drever, J. L. Hall, F. V. Kowalski, J. Hough, G. M. Ford, A. J. Munley, and H. Ward, Appl. Phys. B: Photophys. Laser Chem. **B31**, 97 (1983).
[26] J. Camp (private communication).
[27] D. I. Robertson, P. McNamara, H. Ward, and J. Hough, Class. Quantum Grav. **14**, 1575 (1997).
[28] P. L. Bender, J. L. Hall, J. Ye, and W. M. Klipstein, Space Sci. Rev. **108**, 377 (2003).
[29] E. Morrison, B. J. Meers, D. I. Robertson, and H. Ward, Appl. Opt. **33**, 5037 (1994).
[30] D. J. Jones, S. A. Diddams, J. K. Ranka, A. Stentz, R. S. Windeler, J. L. Hall, and S. T. Cundiff, Science **288**, 635 (2000).
[31] S. Nagano *et al.*, Rev. Sci. Instrum. **73**, 2136 (2002).
[32] T. Kubo-oka (private communication).
[33] G. Ghosh, *Handbook of Thermo-Optic Coefficients of Optical Materials with Applications*, (Academic, San Diego, 1998).
[34] S. Seel, R. Storz, G. Ruoso, J. Mlynek, and S. Schiller, Phys. Rev. Lett. **78**, 4741 (1997).